Photochemical & Photobiological Sciences

PAPER

View Article Online
View Journal | View Issue

Cite this: *Photochem. Photobiol. Sci.*, 2016, **15**, 1347

Sonochemical/hydration–dehydration synthesis of Pt–TiO_2 NPs/decorated carbon nanotubes with enhanced photocatalytic hydrogen production activity

Firas H. Abdulrazzak,[a] Falah H. Hussein,[b] Ayad F. Alkaim,*[c,d] Irina Ivanova,[d] Alexei V. Emeline[e] and Detlef W. Bahnemann[d,e]

Received 3rd July 2016,
Accepted 19th September 2016

DOI: 10.1039/c6pp00240d

www.rsc.org/pps

Modified Pt–TiO_2 NPs/decorated carbon nanotubes were synthesized utilizing sonochemical/hydration–dehydration techniques. Pt was loaded on TiO_2 by a photodeposition method keeping in mind the end goal to achieve electron–hole pair separation and promote the surface reaction. The morphological and basic properties of Pt–TiO_2/fCNTs were investigated by field emission scanning electron microscopy (FESEM), high resolution transmission electron microscopy (HRTEM), powder X-ray diffraction (XRD), UV–vis diffuse reflectance spectroscopy (DRS), photoluminescence (PL) and Raman spectroscopy. The selected area electron diffraction (SAED) patterns of Pt–TiO_2/fCNTs were obtained utilizing TEM-based energy dispersive X-ray spectroscopy (EDXS) analysis. It was found that the TiO_2 nanoparticles were uniformly distributed on the fCNTs, and the Pt particles were decorated on the surface of TiO_2/fCNTs. The photocatalytic hydrogen production activity of the $Pt_{(0.5\%)}$–TiO_2/$fCNTs_{(0.5\%)}$ nanoparticle composites was investigated using a sacrificial agent methanol solution. Pt-loaded TiO_2 demonstrated a hydrogen evolution rate around 20 times that of TiO_2/$fCNTs_{(0.5\%)}$ (fSWCNTs, fMWCNTs). When compared with platinized TiO_2 in methanol, which was utilized as a control material, Pt–TiO_2/fCNTs demonstrated an almost 2-fold increment in hydrogen generation.

1. Introduction

Photocatalytic water splitting for hydrogen production through semiconductor photocatalysts and light irradiation has attracted a great deal of attention as it is a promising technique to solve the energy crisis in future. Photocatalytic water splitting[1] and photocatalytic reforming of biomass[2,3] are two promising strategies for maintainable generation of H_2. The second strategy, specifically, joins synchronous H_2 generation and biomass oxidation.[4–7] The major advantage is that H_2 can be productively delivered by photocatalytic degradation of organic compounds present in aqueous media under mild conditions, with simultaneous treatment of industrial wastes or by-products.[8] The photocatalytic process turns out to be significantly more attractive if solar energy can be utilized as the light source, being at an applicable angle particularly in countries with high insolation levels.

TiO_2 stands out amongst the most encouraging impetuses due to its simple accessibility, long-term stability and non-toxicity.[9] Nonetheless, charge recombination as a rule prompts a low quantum productivity of TiO_2. To determine this issue, numerous methodologies have been proposed to improve the photoactivity of TiO_2, such as loading with noble metal[10] or investigating CNTs as a coupling material with TiO_2.[11] In a variety of scientific fields, carbon nanotubes (CNTs) have warranted huge consideration due to their unique structural, chemical, thermal, and electrical properties[12] and are used in our nanoparticle framework design.

Several recent studies have investigated the utility of coupling TiO_2 to carbon materials, such as carbon nanotubes (CNTs), as an effective way to prevent the aggregation of oxide particles, leading to increased rates of photocatalytic oxidation of pollutants, or to decrease the rate of electron–hole recombination[13–15] by acting as sinks for photogenerated electrons in TiO_2,[16,17] due to the favourable energetics of their electronic band structures, and they have been demonstrated

[a]*Chemistry Department, College of Education for Pure Sciences, Diyala University, Diyala, Iraq*
[b]*College of Pharmacy, Babylon University, Hilla, Iraq*
[c]*Department of Chemistry, College of Science for Women, Babylon University, Hilla, Iraq*
[d]*Institut für Technische Chemie, Leibniz Universität Hannover, Callinstrasse 3, D-30167 Hannover, Germany. E-mail: alkaim@iftc.uni-hannover.de*
[e]*Laboratory "Photoactive Nanocomposite Materials", Saint-Petersburg State University, Ulyanovskaya str. 1, Peterhof, Saint-Petersburg 198504, Russia*

to have a helpful impact on the photocatalytic activity of H_2 production, by actuating synergies between the metal oxide and the carbon phase.[8,18–20] For example, multi-walled carbon nanotubes (MWCNTs)[9,21–23] and single-walled carbon nanotubes (SWCNTs)[11,24] have been investigated to couple with TiO_2, and the subsequent photoactivities are without a doubt moved forward.

The accessible library of nanostructured catalysts has likewise proven that the combination of three nanomaterials represents a powerful strategy to increase more profoundly the various processes taking place during photocatalysis and, eventually, to increase the efficiency of energy conversion processes.[25–29] Interestingly, with simple composites, ternary hybrid composites offer the key advantage of intimate interfaces, namely facilitation of charge/energy transfer, which causes an increased lifetime of charge carriers through spatial separation of photoexcited electron–hole pairs.[30]

In the present work, Pt–TiO_2 NPs/decorated carbon nanotube (fMWCNTs, fSWCNTs) nanocomposite materials are synthesized using a new method by a sonochemical/hydration–dehydration process, and are deliberately investigated by field emission scanning electron microscopy (FESEM), high resolution transmission electron microscopy (HRTEM), energy dispersive X-ray spectroscopy (EDXS), X-ray diffraction (XRD), UV–vis diffuse reflectance spectroscopy (DRS), photoluminescence (PL), and Raman spectroscopy. The Pt–TiO_2/fCNTs (fMWCNTs, fSWCNTs) composite materials were investigated by measuring the photocatalytic production of H_2 from biomass-containing aqueous solutions, namely from methanol either by Pt–TiO_2/fCNTs nanocomposites, or by testing the *in situ* injection addition of Pt to the binary composite TiO_2/fCNTs during the reaction of methanol dehydrogenation as a comparative study.

2. Experimental

2.1 Materials

The MWCNTs and SWCNTs used in this study were purchased from ALDRICH. According to the product specifications, the two compounds were fabricated by chemical vapor deposition (CVD). The SWCNTs consist of more than 90% carbon and are 77% SWCNTs, with a diameter of 0.7–1.1 nm, while the MWCNTs are 95% carbon nanotubes with a mode diameter of 4.5 nm. The metal salt precursor, namely dihydrogen hexachloro palatinate (IV) hexahydrate ($H_2PtCl_6{\cdot}6H_2O$), was supplied by Alfa Aesar. Nitric acid (65 wt% HNO_3) and sulfuric acid (37 wt% H_2SO_4) were obtained from Fluka and Sigma-Aldrich, respectively.

2.2. Functionalization of carbon nanotubes

0.2 g of CNTs (MWCNTs, SWCNTs) was placed in a 500 mL conical flask equipped with a condenser, and 150 mL of $HNO_3 : H_2SO_4$ (1 : 2) with a concentration of 10 mol L^{-1} was added. The mixture was activated under magnetic stirring and sonicated for 2 h at 30 °C, and then this solution was heated to 70 °C for 8 h without stirring. Then the recovered CNTs were washed several times with distilled water up to neutral pH, and then dried at 383 K overnight. This oxidative treatment is very important to help remove amorphous carbon and metallic impurities from the as-produced CNTs,[31] and furthermore to increase the atomic oxygen concentration and the distribution of hydroxyl, carbonyl and carboxylic acid groups.[32]

2.3. Preparation of Pt–TiO_2/fCNTs composites

The TiO_2 used to prepare the Pt–TiO_2/fCNTs composites has been produced in our laboratory through a hydrothermal method.[10]

Pt/TiO_2 was prepared by the photodeposition method as follows: 1 g of TiO_2 nanoparticles photocatalyst was suspended by stirring in 100 mL aqueous solution containing the desired concentration of H_2PtCl_6 to obtain a 0.5 wt% Pt-loaded TiO_2 photocatalyst. The resulting solution was irradiated with UV(A) light employing a Philips Fluorescence Hg lamp (illumination intensity: 1.0 mW cm^{-2}) for 2 h under an Ar atmosphere. Afterwards, 1 mL methanol was injected into the solution followed by further illumination for 10 h. The obtained powder was separated by centrifugation, washed with water, and dried at 100 °C for 12 h.[33] The composites of Pt–TiO_2/fCNTs were prepared firstly by sonicating the solution followed by simple evaporation and drying (hydration/dehydration method) adapted from procedures described in the literature.[16,34] First, approximately 50 mg fCNTs was dispersed in water in a 100 mL beaker and sonicated for 60 min, and the fCNTs content was fixed at 0.5 wt%. Pt/TiO_2 nanoparticles were added to the suspension while stirring, and the suspension containing fCNTs (fSWCNTs, fMWCNTs) and Pt/TiO_2 nanoparticles was heated to 80 °C until complete evaporation of water, and the resulting composites were dried overnight in an oven at 100 °C to avoid any physicochemical change of the fCNTs (fSWCNTs, fMWCNTs) that occurs at higher temperatures in the presence of oxygen.

2.4 Photocatalytic activity for H_2 production

The photocatalytic hydrogen production runs were carried out in an experimental setup comprising of a gas supply, a mass flow controller, and a 100 cm^3 double-jacket quartz glass photoreactor connected to a quadrupole mass spectrometer (QMS) for gas analysis (Hiden HPR-20) as schematically shown in Fig. 1.[35] The system is continuously purged with Ar as the carrier gas, whereby the Ar flow is controlled by a mass flow controller (MFC). In a standard run, 0.05 g of $Pt_{(0.5\%)}/TiO_2$, $TiO_2/fSWCNTs_{(0.5\%)}$, $TiO_2/fMWCNTs_{(0.5\%)}$, $Pt_{(0.5\%)}$–TiO_2/$fSWNTs_{(0.5\%)}$ and $Pt_{(0.5\%)}$–$TiO_2/fMWCNTs_{(0.5\%)}$ was suspended in 60 mL of an aqueous methanol solution (5 mM) by sonication. The suspension was transferred into the photoreactor and purged with Ar for 30 min to evacuate disintegrated O_2. After that, the reactor was connected to the mass flow controller and to the Q/C capillary sampling inlet of the QMS through metal flanges and adapters. To remove the air in the headspace of the reactor, an Ar gas stream was consistently flown through the reactor before irradiation, until no traces of molecular oxygen or nitrogen could be distinguished by the QMS.

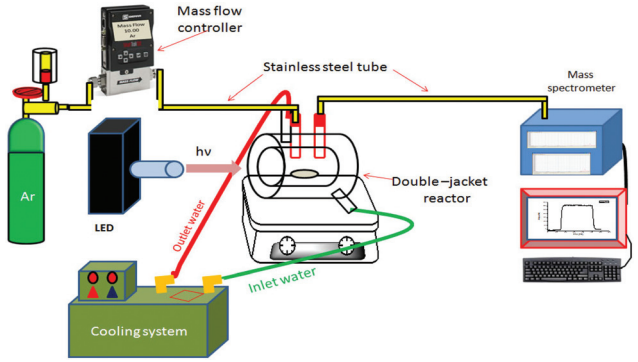

Fig. 1 Continuous flow experimental setup for photocatalytic hydrogen production measurements.

The Ar gas flow rate through the reactor was kept constant at 10 cm^3 min^{-1} during the photocatalytic tests. The inlet flow rate/gas consumption by the QMS is 1 cm^3 min^{-1} and the excess gas is directed towards the exhaust. The sampling rate of the QMS is in the millisecond time range, thus allowing fast tracking of the reaction. After stabilization of the system background, the reactor was irradiated from the outside utilizing collimated UV light of a strong 365 nm LED (Thorlabs/USA). For quantitative analysis of H_2, the QMS was calibrated employing standard diluted H_2, in Ar (Linde Gas, Germany).

2.5. Analytical instruments

The morphological analysis of TiO_2, TiO_2/fSWCNTs$_{(0.5\%)}$, TiO_2/fMWCNTs$_{(0.5\%)}$, Pt$_{(0.5\%)}$/TiO_2, Pt$_{(0.5\%)}$–TiO_2/fSWCNTs$_{(0.5\%)}$, and Pt$_{(0.5\%)}$–TiO_2/fMWCNTs$_{(0.5\%)}$ was done using different techniques.

Powder X-ray diffraction (XRD) was performed in a Bruker AXS D4 Endeavour diffractometer using a reflection geometry with fixed divergence slits, Cu K$\alpha_{1,2}$ radiation, and a nickel filter. Three thousand data points were collected with a step width of 0.02° per step in the 2θ range from 20 to 80°. To determine the particle size, and element type, field emission scanning electron microscopy (FESEM) measurements were carried out on a JEOL JSM-6700F field emission instrument using a secondary electron detector (SE) at an accelerating voltage of 2 kV, and HRTEM and energy dispersive X-ray spectroscopy (EDXS) were performed at 200 kV with an ultrahigh resolution pole piece (CS = 0.5 mm), which provides a point resolution better than 0.19 nm. Raman spectra of the samples were recorded in the 45–2300 cm^{-1} spectral region at ambient temperature using a SENTERRA Raman spectrometer (Bruker) with a resolution of 1 cm^{-1} (the excitation laser wavelength was 532 nm. Data were collected using an 1800 grating in the Raman shift range from 0 to 2300 cm^{-1}, and the laser beam power was 20 mW).

Photoluminescence (PL) spectroscopy of the synthesized composites was done at room temperature on a Hitachi F2500 spectrofluorometer using a Xe lamp with an excitation wavelength of 355 nm.

The bandgap energy of the catalysts was measured using diffuse reflectance spectroscopy (DRS). The reflectance spectra of the samples within the 200–700 nm wavelength range were recorded with a UV–vis spectrophotometer (Varian Cary 100) equipped with a Labsphere integrating sphere diffuse reflectance accessory and using $BaSO_4$ as the reference material. UV–vis spectra were performed in the diffuse reflectance mode (R) and transformed to the Kubelka–Munk function F(R) to separate the extent of light absorption from scattering. Furthermore the bandgap values were obtained from the plot of the modified Kubelka–Munk function $(F(R)E)^{1/2}$) *versus* the energy of the absorbed light E:[36]

$$F(R)E^{1/2} = \left(\frac{(1-R)^2}{2R} \times h\nu\right)^{1/2}$$

The Brunauer–Emmett–Teller (BET) surface area of the prepared nanocomposites was analysed by nitrogen adsorption using a Micromeritics ASAP 2020 nitrogen adsorption apparatus (USA). All measurements for the surface area were repeated three times and the average of these measurements was calculated.

3. Results and discussion

3.1 Catalyst characterization

XRD was used to characterize the difference of phase structures and average crystallite sizes of the samples Fig. 2 shows comparison of XRD patterns of fCNTs (fSWCNTs, fMWCNTs), TiO_2/fCNTs$_{(0.5\%)}$ (fSWCNTs, fMWCNTs), Pt/TiO_2, and Pt$_{(0.5\%)}$/TiO_2/fCNTs$_{(0.5\%)}$ (fSWCNTs, fMWCNTs) composites. Also, Fig. 2 shows XRD patterns of Pt–TiO_2/fCNTs composite that has diffraction peaks of TiO_2 and Pt/TiO_2. The peak at 2θ value of 25 is broad indicating (0 0 2) phase of fCNTs and (1 0 1) phase of TiO_2 have overlapped. Otherwise, no apparent peaks for fCNTs or Pt are observed because of its lower loading content and weak crystallization[37] However, the existence of

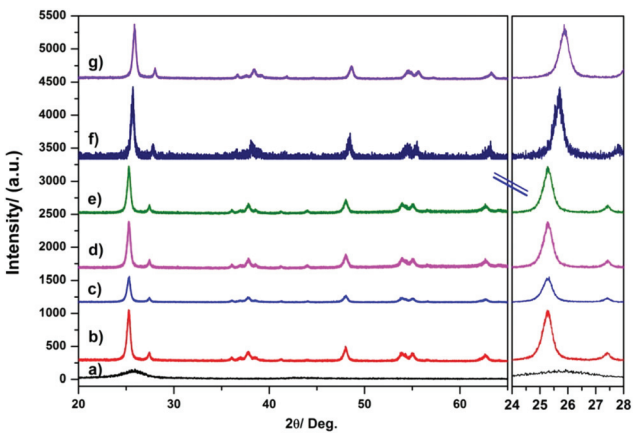

Fig. 2 X-ray diffraction of (a) pure TiO_2, (b) pure CNTs (fMWCNTs), (c) Pt/TiO_2, (d) TiO_2/fMWCNTs, (e) TiO_2/fSWCNTs, (f) Pt–TiO_2/fSWCNTs, and (g) Pt–TiO_2/fMWCNTs.

fCNTs can be clearly identified by Raman analysis as discussed later.

There are diffraction peaks corresponding to fCNTs; the two peaks at 26.5° and 43.5° can be attributed to reflection from C(0 0 2) and C(1 0 0) facets.[38,39] The phases of the synthesized TiO_2 anatase structure are well known. These features are observed in the XRD spectra for the Pt–TiO_2 and Pt–TiO_2/fCNTs (fSWCNTs, fMWCNTs) nanoparticle composites. In addition, the peaks corresponding to the Pt component have not been observed; moreover as shown in Fig. 2, the peaks related to fCNTs are absent from the XRD patterns caused by the overlap of the (0 0 2) peak of fCNTs and (1 0 1) phase of TiO_2 as well, because of the amorphous structure of the impregnated fibers and because of the fact that the intense graphite peaks (0 0 2) overlap with the TiO_2 anatase (0 0 1) reflections, which thus obscure the graphite peaks because the amount of TiO_2 that is present in the material is much larger than the amount of fCNTs.[40] The crystal sizes of all samples also can be estimated using the Scherrer equation. Taking the peak of the (101) planes into account, the average crystalline sizes of the samples are illustrated in Table 1.

Table 1 Physicochemical properties of the synthesized ternary nanocomposites

Material label	Surface area/m^2 g^{-1}	Crystal size/nm	Bandgap/eV
fMWCNTs	286.4	7.64	—
fSWCNTs	570.2	6.52	—
TiO_2	113.1	11.44	3.11
Pt/fMWCNTs	92.77	9.71	—
Pt/fSWCNTs	105.34	8.42	—
Pt/TiO_2	107.41	12.72	2.85
Pt–TiO_2/fMWCNTs	111.45	13.61	2.73
Pt–TiO_2/fSWCNTs	118.23	14.32	2.61

The nano-surface structures of the Pt–TiO_2/fCNTs (MWCNTs) nanoparticle composites were characterized by FESEM and HRTEM-based EDXS analysis. As shown in Fig. 3(a) and (b) with images of different magnifications, fCNTs (fMWCNTs) were coated with well-dispersed Pt/TiO_2 nanoparticles, and their distribution was uniform. The dispersion of small particles is optimal for surface catalysis as this can provide more reactive sites for the reactants than aggregated particles.[29] HRTEM was used to further examine the surface structure of the Pt–TiO_2/fMWCNTs nanoparticle composites as shown in Fig. 3(c) and (d). The images confirm that the surface of the fCNTs has been uniformly decorated with Pt/TiO_2 particles of size ~10–20 nm. Also, the Pt–TiO_2/fCNTs nanoparticle composites were found to be covered with aciniform structures of Pt–TiO_2, as shown in Fig. 3(c) and (d).

The HRTEM images (Fig. 3(c) and (d)) of Pt–TiO_2/fMWCNTs show that some of the Pt/TiO_2 nanoparticles deposit on the fMWCNTs, and it is clear when Fig. 3(c) is magnified as shown in Fig. 3(d), because its surface contains an abundance of oxygen-containing groups, which is beneficial for preferential heterogeneous nucleation and growth of nanoparticles. The chemical composition of the sample Pt–TiO_2/fMWCNTs was determined by energy dispersive X-ray spectroscopy (EDXS). The EDXS spectrum (Fig. 4) confirms that the sample consists of C, O, Ti and Pt elements, as expected.

Fig. 5 summarizes the Raman spectra of the Pt–TiO_2/fCNTs (fMWCNTs, fSWCNTs) composites. The characteristic Raman modes of the anatase TiO_2 phase were readily detected at 150 cm^{-1} (E_g), 395.1 cm^{-1} (B_{1g}), 512.5 cm^{-1} (A_{1g} + B_{1g}), and 636.7 cm^{-1} (E_g) due to anatase as well as the very low intensity

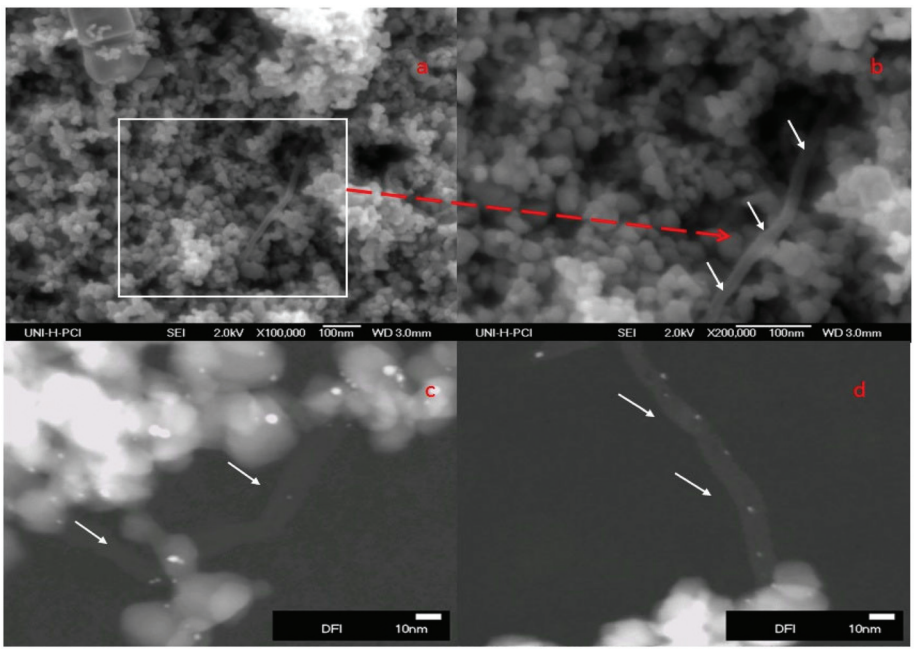

Fig. 3 FESEM images of $Pt_{(0.5\%)}/TiO_2$–$fMWCNTs_{(0.5\%)}$ (a and b); HRTEM images of $Pt_{(0.5\%)}$–TiO_2/$fMWCNTs_{(0.5\%)}$ (c and d).

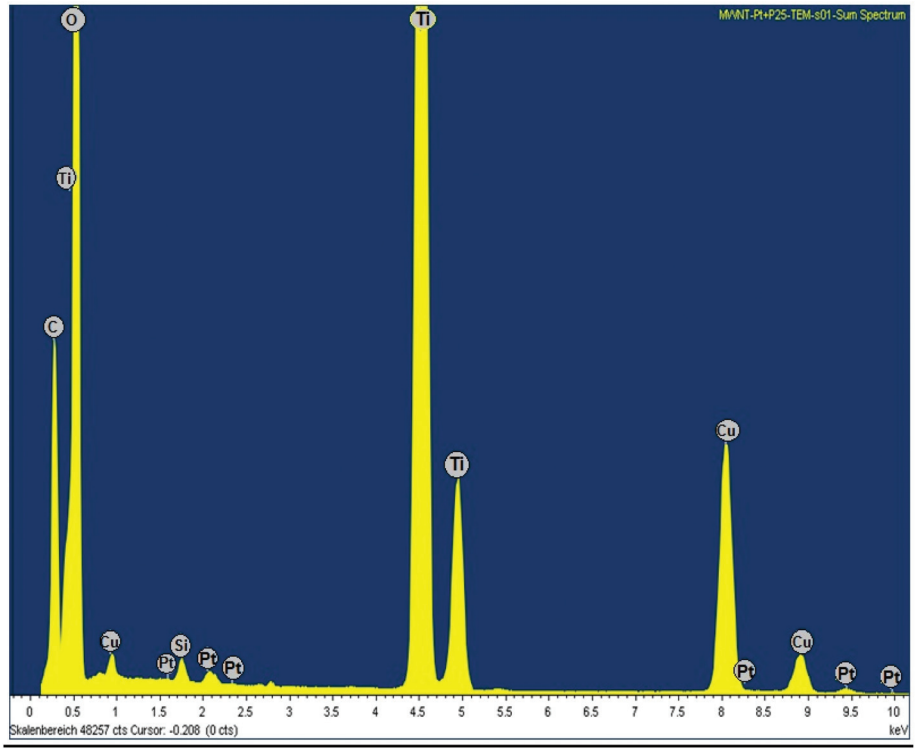

Fig. 4 Energy dispersive X-ray spectroscopy (EDXS) of Pt–TiO_2/fMWCNTs.

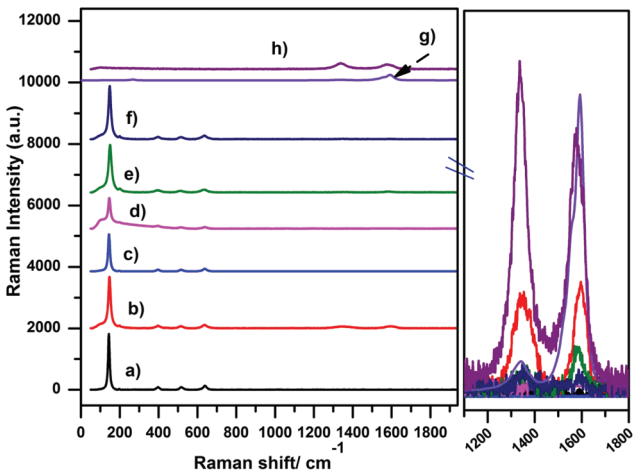

Fig. 5 Typical Raman spectra of (a) TiO_2, (b) TiO_2/fSWCNTs, (c) TiO_2/fMWCNTs, (d) Pt/TiO_2, (e) $Pt_{(0.5\%)}$–TiO_2/$fSWCNTs_{(0.5\%)}$, (f) $Pt_{(0.5\%)}$–TiO_2/$fMWCNTs_{(0.5\%)}$, (g) fSWCNTs, and (h) fMWCNTs nanocomposites.

235 cm^{-1} (A_{1g}) band ascribed to rutile.[25,41] As for the fCNTs (fSWCNTs, fMWCNTs), two typical Raman bands are observed (Fig. 5(g) and (h)); one at 1582 cm^{-1}, which is indicative of the G band (Raman-allowed E_{2g} mode) characterizing the crystalline nature of the fCNTs, together with a band at 1332 cm^{-1} (D band, assigned to the A_{1g} phonon mode) originating from the disordered sp^2 carbon[42,43]

On the other hand, TiO_2 causes an increase in the atomic disorder in the TiO_2/fCNTs system through the creation of defects, as depicted in the inset of Fig. 5. This effect could be attributed to the ultrasonic treatment during the synthesis and the interaction between acid-treated fCNTs and TiO_2 or by the effect of TiO_2/fCNTs platinized by the photodeposition process.[44]

No significant change in the position and widths of these bands is noted. Instead, the D/G intensity ratio undergoes a slight increase with respect to the value measured in TiO_2/fCNTs or $Pt_{(0.5\%)}$–TiO_2/$fCNTs_{(0.5\%)}$ as is clear in Fig. 5, while the relative intensity of the Raman TiO_2 modes changes with varying the CNTs or Pt loading.

As previously pointed out,[45,46] Raman analysis demonstrates that the addition of TiO_2 or Pt/TiO_2 to the fCNTs leads to an enhancement of the D/G integrated intensity ratio, *i.e.* of the structural disorder of the graphitic network. Comparing the spectra of TiO_2/fCNTs and $Pt_{(0.5\%)}$–TiO_2/$fCNTs_{(0.5\%)}$ (Fig. 5(d)–(f)), a further slight increase can be noted in all the samples, caused by the anchoring of the TiO_2 NPs on oxygenated groups introduced during fCNTs surface functionalization.[47]

Photoluminescence is a powerful tool to probe the electron–hole pair formation and their recombination at surfaces.[48,49] The PL measurements were carried out with pure TiO_2, Pt/TiO_2 and with loading and unloading Pt on the TiO_2/fCNTs (fSWCNTs, fMWCNTs) composites, as shown in Fig. 6. A maximum peak around 400 nm is observed, which is due to the bandgap transition of TiO_2. The small peaks in the wavelength region of 450–475 nm are assigned to excitonic PL resulting from surface defects/vacancies.[49] The PL spectra can be attributed

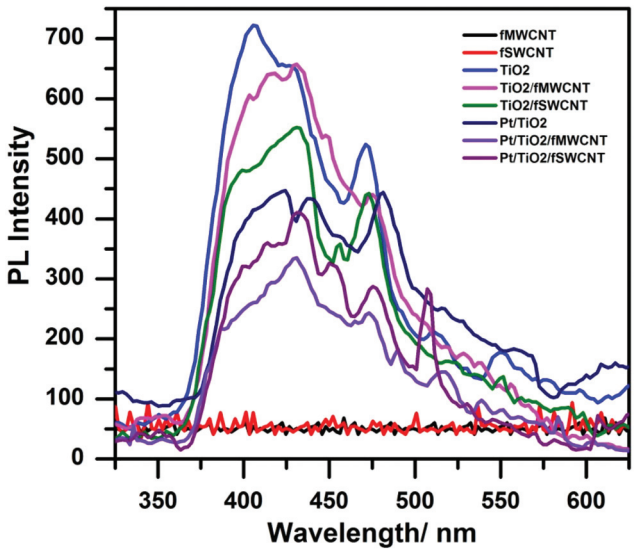

Fig. 6 Photoluminescence (PL) plots of the prepared nanocomposites.

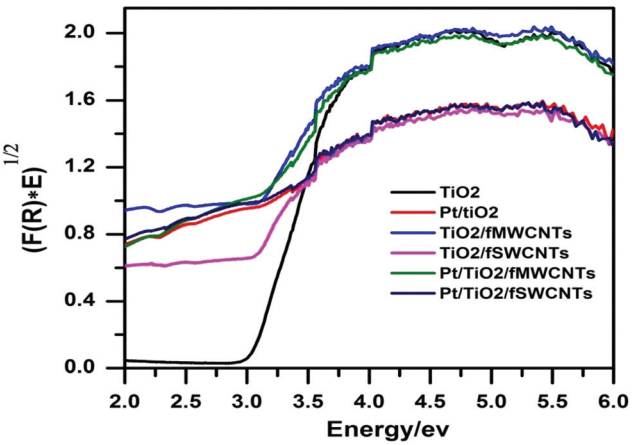

Fig. 7 Plot of transferred Kubelka–Munk function *versus* energy of the light absorbed of the prepared nanocomposites.

to the recombination process of the electron–hole pair at the surface.[50] An overall reduction in PL intensity was observed with either fCNTs (fMWCNTs, fSWCNTs) or Pt photodeposited on the TiO_2 surface. Furthermore a higher reduction was detected in the presence of both fCNTs (fSWCNTs, fSWCNTs) and Pt on the TiO_2 surface as shown in Fig. 6. Therefore, Pt–TiO_2/fCNTs has a lower recombination rate of electron–hole pairs compared with that of Pt/TiO_2 or TiO_2/fCNTs.

The decrease in PL intensity for the composite Pt–TiO_2/fCNTs indicates transfer of photogenerated electrons from TiO_2 to fCNTs and Pt, thus reducing the recombination probability and lowering the PL intensity.[51] This may be one reason why the Pt–TiO_2/fCNTs showed a higher photoactivity of hydrogen evolution than Pt/TiO_2 or TiO_2/fCNTs (fMWCNTs, fSWCNTs) did.[52] Also the reduction is greater in the fSWCNTs composites than in the fMWCNTs composite, which is consistent with the evidence of better attachment for the Pt–TiO_2/fSWCNTs composite than for the Pt–TiO_2/fMWCNTs composite. As expected, no luminescence was observed in the range of 400–650 nm for the fCNTs (fSWCNTs, fMWCNTs).[16]

In order to elucidate the optical response and to determine the bandgaps of the nanocomposite samples, UV–visible diffuse reflectance spectroscopy (UV–vis DRS) was carried out. The bandgap energy (E_g) of these samples was estimated from the plot of the square root of the Kubelka–Munk function *versus* photon energy as shown in Fig. 7. The characteristic spectrum of the fundamental absorption edge at 370 nm (with a 3.1 eV band edge) was clearly observed. The Pt–TiO_2/fCNTs nanocomposite displayed stronger absorption than TiO_2/CNTs did, and the band edge of Pt–TiO_2/fCNTs is 2.73 and 2.61 eV respectively, and the results are illustrated in Table 1. It is suggested that the surface electric charge of the nanocomposite increases due to the fCNTs introduction, which may lead to modifications of the procedure of electron–hole pair formation during visible light irradiation.[53] Also the Pt–TiO_2/fCNTs photocatalysts probably exhibit surface plasmon resonance (SPR) due to the presence of Pt particles,[54] or ascribed to low-energy transitions between the valence band of TiO_2 and localized energy levels introduced to the bandgap by deposited metal clusters.[33]

The surface area for pristine and modified TiO_2 was measured using the Brunauer–Emmett–Teller method and the results are listed in Table 1. The results show that the Pt–TiO_2/fCNTs framework has a larger specific surface area than that of Pt/fCNTs. Since there is more surface area with TiO_2, it is expected that Pt shows a superior dispersion on the TiO_2/fCNTs support, leaving more area exposed for the surface reaction to take place.[44]

3.2. Photocatalytic hydrogen production

The activities of the composites with 0.5% fCNTs (fSWCNTs, fMWCNTs) loading on Pt/TiO_2 were tested in the photocatalytic evolution of hydrogen from aqueous methanol solutions. Blank experiments showed no appreciable H_2 evolution in the absence of either irradiation light or photocatalysts of Pt–TiO_2/fCNTs, and also no activity was observed over pure fCNTs or TiO_2 in the presence of light, which may be attributed to the presence of overpotential in the production of H_2 on the TiO_2 surface and the fast backward recombination of hydrogen and oxygen into water, making TiO_2 less active in photocatalytic water splitting due to the high recombination between CB electrons and VB holes in pure TiO_2.

Fig. 8 displays the photocatalytic activities for H_2 evolution over Pt/TiO_2, TiO_2/fSWCNTs, TiO_2/fMWCNTs, Pt–TiO_2/fSWCNTs, and Pt–TiO_2/fMWCNTs. All the samples were irradiated for 3 hours. It can be seen clearly from Fig. 8 that $Pt_{(0.5\%)}$–TiO_2/$fCNTs_{(0.5\%)}$ exhibits a significant enhancement in H_2 evolution as compared to TiO_2/fCNTs (fSWCNTs, fMWCNTs) and even Pt/TiO_2.

Thus an increase in the photocatalytic performance of Pt–TiO_2/fCNTs is mainly due to photodeposition of Pt nanoparticles. It is well known that the deposition of noble metals

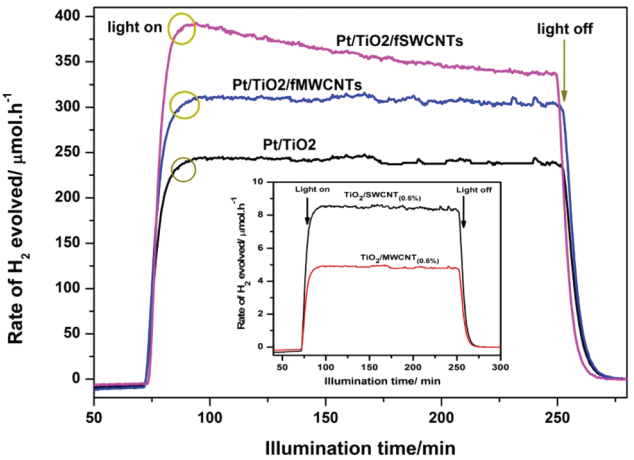

Fig. 8 Timeline of nanocomposite photocatalytic H_2 evolution from methanol aqueous solution (timeline of photocatalytic H_2 evolution from methanol aqueous solution in the presence of TiO_2/fCNTs (fSWCNTs, fMWCNTs). Experimental conditions: methanol conc. 5 mM, light intensity 40 mW cm^{-2}, mass of catalyst 50 mg, and irradiation time 3 h.

usually enhances the separation and prolongs the lifetime of photogenerated electrons and holes (e^-–h^+), resulting in the improved photocatalytic activity.[55] This leads to an increase of photocatalytic hydrogen generation, which is attributed to atomic Pt and results in an increase of electron sinks, thus improving the photocatalyst activity with moderate reaction rates.[56]

Comparative experiments were used to understand the effect of the position of Pt on the reaction by (*in situ*) injection of Pt into TiO_2/fCNTs photocatalysts with the same composition ratio as that prepared in the photodeposition method. Fig. 9 shows that *in situ* injection of Pt ions to TiO_2/fSWCNTs achieved a rate of 254 µmol h^{-1}, which is higher than that for

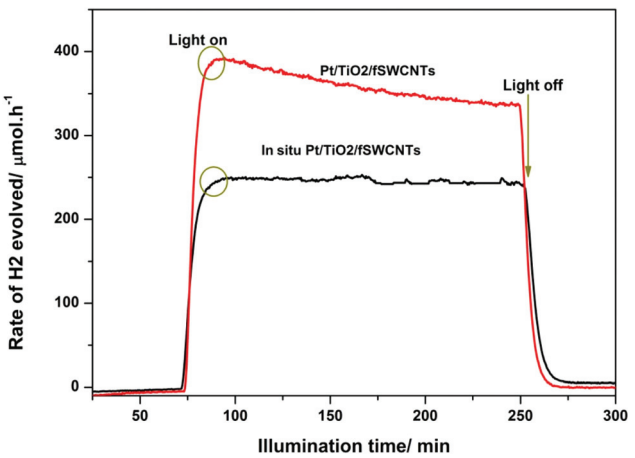

Fig. 9 Timeline of photocatalytic H_2 evolution from methanol aqueous solution in a comparative *in situ* study. Experimental conditions: methanol conc. 5 mM, light intensity 40 mW cm^{-2}, mass of catalyst 50 mg, and irradiation time 3 h.

TiO_2/fCNTs (fSWCNTs, fMWCNTs), but lower than that for Pt–TiO_2/fSWCNTs (355 µmol h^{-1}). This demonstrates that the strong interaction between fCNTs and Pt/TiO_2 formed in the sonochemical/hydration–dehydration and photodeposition reaction plays a crucial role in the water reduction process.

All of that confirms two facts, the first being that the addition of fCNTs and Pt simultaneously has an effect that is greater than that from the addition of each of them individually. The second fact is that the synergic roles depend on the nature of distribution and concoctions between Pt with TiO_2 and fCNTs with TiO_2 to form Pt–TiO_2/fCNTs.

3.3. Mechanism for the enhancement of the photocatalytic activity by Pt–TiO_2/fCNTs

It is well known that the light absorption capability of the photocatalyst and separation of photogenerated e^-/h^+ pairs are crucial factors influencing the photoactivity, as well as the formation of a semiconductor–metal junction (Schottky barrier) where there is a space charge separation region. This Schottky barrier will result in the metal possessing an excess negative charge and the semiconductor an excess positive charge.[57] Thus, after TiO_2 absorbs a photon, the excited electron and hole need to be separated and transferred to the surface of TiO_2, to react with corresponding water or sacrificial agents.[58] The excited e^- may migrate into either the metal surface or to the nano-cylinder of fCNTs causing a reduction in the chance of recombination of e^-/h^+. Meanwhile upon light irradiation, the photogenerated electrons are excited from the valence band (VB) to the conduction band (CB) leaving positive holes in the VB. The holes accumulated at the valence band oxidize methanol to give a methoxide ion (radical species) and a proton.

The excited electrons migrate to the Pt nanoparticles which act as electron traps then reduce the protons to produce H_2. The general functions of Pt and fCNTs can be represented in two probabilities: the first is related to the Pt nanoparticles that are photodeposited on TiO_2 forming a Schottky barrier at the Pt–TiO_2 interface based on the difference between the Pt work-function (5.7 eV)[59] and the electron affinity (χ = 3.8 eV) of the TiO_2 conduction band. The second probability may be due to the excited electrons transferred from the low electron conductivity of the TiO_2 phase to the high electron conductivity of the carbon phase in the TiO_2/CNTs composites.[60] Besides, well mixed TiO_2 particles with the fCNTs network create local potential differences in the TiO_2 phase which spread through the sample, resulting in more effective e^-/h^+ separation within the entire sample.[61] The work-functions of fCNTs (fSWCNTs, fMWCNTs) are about 4.8 and 4.3 eV respectively[62] when fCNTs were added, and charge transfer from the TiO_2 conduction band (E_{CB} = 0.5 V *versus* normal hydrogen electrode (NHE)) to the SWCNTs conduction band (E_{CB} = 0.3 V *versus* NHE) is therefore energetically favourable for all types of CNTs.[63]

In both cases of the suggested mechanism, the injected electrons will assist as H_2 evolution sites to reduce water molecules. Meanwhile, methanol (donor) is oxidized by donating the electrons to Pt or fCNTs. As shown in Fig. 9, the fSWCNTs

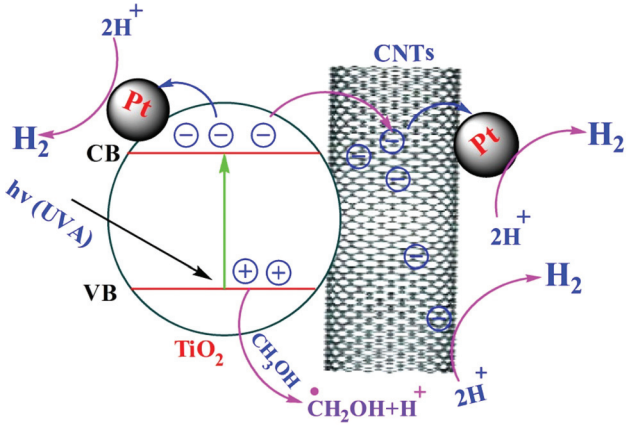

Fig. 10 Schematic diagram for the mechanism of the reactions for the ternary composite (Pt–TiO_2/fCNTs).

have higher activities compared to those of fMWCNTs, and the same results have been found in previously published work.[63] The SWCNTs are more favourable for charge transfer[64] as compared to the MWCNTs, which may be due to them acting as mid-gap bands, causing the possible multi-electron–hole pair (exciton) generation by absorption of single high energy photons in the UV region across these multiple low energy bandgaps.[65] Meanwhile for MWCNTs, the origin of the photoconductivity is less clear.[66] Yao *et al.*[16] reported that the TiO_2/fSWCNTs composite demonstrated a higher photocatalytic activity than that of the TiO_2/fMWCNTs composite under UV light irradiation. This occurrence is believed to be related to the higher degree of interphase contact that can be achieved at the TiO_2 surface with the bundles of small individual SWCNTs.[67] Woan *et al.* reported that a hydrothermally synthesized SWCNT–TiO_2 hybrid showed superior enhancement in the photocatalytic degradation of pirimicarb compared with that of MWCNTs/TiO_2,[19] which is attributed to the higher separation efficiency of photogenerated carriers that was achieved because of the high conductivity of SWCNTs.[68] All of these explanations and reasons lead to the ternary mechanism in Fig. 10, which produces H_2 gas in three routes, with the probabilities for Pt in two lines while there is one line for fCNTs. The practical proof of these results was accrued when an *in situ* experiment was done which mostly localized the Pt on the surfaces of fCNTs, and showed the percent of Pt that was localized on the surface of TiO_2.

4. Conclusions

In summary, a $Pt_{(0.5\%)}$–TiO_2/$fCNTs_{(0.5\%)}$ ternary hybrid has been successfully synthesized by a new sonochemical/hydration–dehydration route. The results show that Pt/TiO_2 was more active than the binary composites TiO_2/fCNTs. Among the various nanostructures (Pt–TiO_2/fSWCNTs, Pt–TiO_2/fMWCNTs, Pt/TiO_2, and TiO_2/fCNTs), Pt–TiO_2/fSWCNTs shows the maximum photocatalytic H_2 production rate (355 μmol h^{-1}) due to having the best charge carrier transfer and separation, caused by a reduction in the recombination rate of electron–hole pairs compared with the other nanocomposites. Furthermore, the results show that the photocatalytic activity of the ternary hybrid catalysts is highly dependent on the type of fCNTs, as investigated in our work, with the activity of fSWCNTs being higher than that of fMWCNTs for hydrogen production. Finally the indicator for this behavior was the *in situ* injection of Pt to the binary composite TiO_2/$fSWCNTs_{(0.5\%)}$, which shows a reduction in activity as compared with $Pt_{(0.5\%)}$/TiO_2 and Pt–TiO_2/SWNTs. Furthermore, photocatalyst-based flexible fCNTs have advantages for industrial application because of the type-dependence of fCNTs which gives a cost-effective co-catalyst for photocatalytic H_2 production.

Acknowledgements

Detlef W. Bahnemann and I. Ivanova acknowledge financial support from the BMBF (Bundesministerium für Bildung und Forschung), research project DuaSol (03SF0482C). The present study was performed within the Project "Establishment of the Laboratory Photoactive Nanocomposite Materials" no. 14. Z50.31.0016 supported by a mega-grant of the Government of the Russian Federation.

References

1 H. Bahruji, M. Bowker, P. R. Davies, L. S. Al-Mazroai, A. Dickinson, J. Greaves, D. James, L. Millard and F. Pedrono, Sustainable H_2 gas production by photocatalysis, *J. Photochem. Photobiol., A*, 2010, **216**, 115–118.
2 D. I. Kondarides, V. M. Daskalaki, A. Patsoura and X. E. Verykios, Hydrogen Production by Photo-Induced Reforming of Biomass Components and Derivatives at Ambient Conditions, *Catal. Lett.*, 2008, **122**, 26–32.
3 A. Speltini, M. Sturini, F. Maraschi, D. Dondi, G. Fisogni, E. Annovazzi, A. Profumo and A. Buttafava, Evaluation of UV-A and solar light photocatalytic hydrogen gas evolution from olive mill wastewater, *Int. J. Hydrogen Energy*, 2015, **40**, 4303–4310.
4 M. Ilie, B. Cojocaru, V. I. Parvulescu and H. Garcia, Improving TiO_2 activity in photo-production of hydrogen from sugar industry wastewaters, *Int. J. Hydrogen Energy*, 2011, **36**, 15509–15518.
5 A. Speltini, M. Sturini, F. Maraschi, D. Dondi, A. Serra, A. Profumo, A. Buttafava and A. Albini, Swine sewage as sacrificial biomass for photocatalytic hydrogen gas production: Explorative study, *Int. J. Hydrogen Energy*, 2014, **39**, 11433–11440.
6 A. Speltini, M. Sturini, D. Dondi, E. Annovazzi, F. Maraschi, V. Caratto, A. Profumo and A. Buttafava, Sunlight-promoted photocatalytic hydrogen gas evolution from water-suspended

cellulose: a systematic study, *Photochem. Photobiol. Sci.*, 2014, **13**, 1410–1419.

7 N. M. Gupta, S. Kelkar and P. Korake, The quenching effect of uranyl species in the photoluminescence emission and visible-light-driven water dissociation activity of CdS and TiO_2 photocatalysts, *Photochem. Photobiol. Sci.*, 2016, **15**, 758–766.

8 C. G. Silva, M. J. Sampaio, R. R. Marques, L. A. Ferreira, P. B. Tavares, A. M. Silva and J. L. Faria, Photocatalytic production of hydrogen from methanol and saccharides using carbon nanotube-TiO_2 catalysts, *Appl. Catal., B*, 2015, **178**, 82–90.

9 Q. Zeng, H. Li, H. Duan, Y. Guo, X. Liu, Y. Zhang and H. Liu, A green method to prepare TiO_2/MWCNT nanocomposites with high photocatalytic activity and insights into the effect of heat treatment on photocatalytic activity, *RSC Adv.*, 2015, **5**, 13430–13436.

10 A. F. Alkaim, T. A. Kandiel, F. H. Hussein, R. Dillert and D. W. Bahnemann, Solvent-free hydrothermal synthesis of anatase TiO_2 nanoparticles with enhanced photocatalytic hydrogen production activity, *Appl. Catal., A*, 2013, **466**, 32–37.

11 C. Bo, P. Tianyou, Z. Xiaohu, M. Jing, L. Kan and Z. Xungao, Synthesis of C60-decorated SWCNTs (C60-d-CNTs) and its TiO_2-based nanocomposite with enhanced photocatalytic activity for hydrogen production, *Dalton Trans.*, 2013, **42**, 3402–3409.

12 R. H. Baughman, A. A. Zakhidov and W. A. de Heer, Carbon Nanotubes–the Route Toward Applications, *Science*, 2002, **297**, 787–792.

13 G. An, W. Ma, Z. Sun, Z. Liu, B. Han, S. Miao, Z. Miao and K. Ding, Preparation of titania/carbon nanotube composites using supercritical ethanol and their photocatalytic activity for phenol degradation under visible light irradiation, *Carbon*, 2007, **45**, 1795–1801.

14 W. Wang, P. Serp, P. Kalck and J. L. Faria, Visible light photodegradation of phenol on MWNT-TiO_2 composite catalysts prepared by a modified sol-gel method, *J. Mol. Catal. A: Chem.*, 2005, **235**, 194–199.

15 G. Zhu, H. Wang, G. Yang, L. Chen, P. Guo and L. Zhang, A facile synthesis of ZnO/CNT hierarchical microsphere composites with enhanced photocatalytic degradation of methylene blue, *RSC Adv.*, 2015, **5**, 72476–72481.

16 Y. Yao, G. Li, S. Ciston, R. M. Lueptow and K. A. Gray, Photoreactive TiO_2/Carbon Nanotube Composites: Synthesis and Reactivity, *Environ. Sci. Technol.*, 2008, **42**, 4952–4957.

17 B. Ahmmad, Y. Kusumoto, S. Somekawa and M. Ikeda, Carbon nanotubes synergistically enhance photocatalytic activity of TiO_2, *Catal. Commun.*, 2008, **9**, 1410–1413.

18 R. Leary and A. Westwood, Carbonaceous nanomaterials for the enhancement of TiO_2 photocatalysis, *Carbon*, 2011, **49**, 741–772.

19 K. Woan, G. Pyrgiotakis and W. Sigmund, Photocatalytic Carbon-Nanotube–TiO_2 Composites, *Adv. Mater.*, 2009, **21**, 2233–2239.

20 C. G. Silva and J. L. Faria, Photocatalytic oxidation of benzene derivatives in aqueous suspensions: Synergic effect induced by the introduction of carbon nanotubes in a TiO_2 matrix, *Appl. Catal., B*, 2010, **101**, 81–89.

21 S. Da Dalt, A. K. Alves, F. A. Berutti and C. P. Bergmann, Designing of TiO_2/MWCNT Nanocomposites for Photocatalytic Degradation of Organic Dye, *Part. Sci. Technol.*, 2015, **33**, 308–313.

22 B. Reti, K. Mogyorosi, A. Dombi and K. Hernadi, Substrate dependent photocatalytic performance of TiO_2/MWCNT photocatalysts, *Appl. Catal., A*, 2014, **469**, 153–158.

23 S. Muduli, W. Lee, V. Dhas, S. Mujawar, M. Dubey, K. Vijayamohanan, S.-H. Han and S. Ogale, Enhanced Conversion Efficiency in Dye-Sensitized Solar Cells Based on Hydrothermally Synthesized TiO_2-MWCNT Nanocomposites, *ACS Appl. Mater. Interfaces*, 2009, **1**, 2030–2035.

24 K. Vajda, K. Mogyorosi, Z. Nemeth, K. Hernadi, L. Forro, A. Magrez and A. Dombi, Photocatalytic activity of TiO_2/SWCNT and TiO_2/MWCNT nanocomposites with different carbon nanotube content, *Phys. Status Solidi B*, 2011, **248**, 2496–2499.

25 M. Mokhtar Mohamed, G. Osman and K. S. Khairou, Fabrication of Ag nanoparticles modified TiO_2/CNT heterostructures for enhanced visible light photocatalytic degradation of organic pollutants and bacteria, *J. Environ. Chem. Eng.*, 2015, **3**, 1847–1859.

26 X. Wang, J. Zhang and H. Zhu, Pt-Au/CNT@TiO_2 as a High-Performance Anode Catalyst for Direct Methanol Fuel Cells, *Chin. J. Catal.*, 2011, **32**, 74–79.

27 M. N. Uddin, M. S. Islam, M. R. Mazumder, M. A. Hossain, M. Elias, I. A. Siddiquey, M. H. Susan, D. K. Saha, M. M. Rahman, A. M. Asiri and S. Hayami, Photocatalytic and antibacterial activity of B/N/Ag co-doped CNT–TiO_2 composite films, *J. Inclusion Phenom. Macrocyclic Chem.*, 2015, **82**, 229–234.

28 M. Sangari, M. Umadevi, J. Mayandi and J. P. Pinheiro, Photocatalytic degradation and antimicrobial applications of F-doped MWCNTs/TiO_2 composites, *Spectrochim. Acta, A*, 2015, **139**, 290–295.

29 Y. Koo, G. Littlejohn, B. Collins, Y. Yun, V. N. Shanov, M. Schulz, D. Pai and J. Sankar, Synthesis and Characterization of Ag-TiO_2-CNT Nanoparticle Composites with High Photocatalytic Activity under Artificial Light, *Composites, Part B*, 2014, **57**, 105–111.

30 A. Moya, A. Cherevan, S. Marchesan, P. Gebhardt, M. Prato, D. Eder and J. J. Vilatela, Oxygen vacancies and interfaces enhancing photocatalytic hydrogen production in mesoporous CNT/TiO_2 hybrids, *Appl. Catal., B*, 2015, **179**, 574–582.

31 C. Bergeret, J. Cousseau, V. Fernandez, J.-Y. Mevellec and S. Lefrant, Spectroscopic evidence of carbon nanotubes' metallic character loss induced by covalent functionalization via nitric acid purification., *J. Phys. Chem. C*, 2008, **112**, 16411–16416.

32 K. A. Wepasnick, B. A. Smith, K. E. Schrote, H. K. Wilson, S. R. Diegelmann and D. H. Fairbrother, Surface and structural characterization of multi-walled carbon nanotubes following different oxidative treatments, *Carbon*, 2011, **49**, 24–36.

33 A. F. Alkaim, R. Dillert and D. W. Bahnemann, Effect of polar and movable (OH or NH2 groups) on the photocatalytic H_2 production of alkyl-alkanolamine: a comparative study, *Environ. Technol.*, 2015, **36**, 2190–2197.

34 S. M. Miranda, G. E. Romanos, V. Likodimos, R. R. N. Marques, E. P. Favvas, F. K. Katsaros, K. L. Stefanopoulos, V. J. P. Vilar, J. L. Faria, P. Falaras and A. N. M. T. Silva, Pore structure, interface properties and photocatalytic efficiency of hydration/dehydration derived TiO_2/CNT composites, *Appl. Catal., B*, 2014, **147**, 65–81.

35 T. A. Kandiel, I. Ivanova and D. W. Bahnemann, Long-term investigation of the photocatalytic hydrogen production on platinized TiO_2: an isotopic study, *Energy Environ. Sci.*, 2014, **7**, 1420–1425.

36 A. A. Ismail, D. W. Bahnemann, I. Bannat and M. Wark, Gold Nanoparticles on Mesoporous Interparticle Networks of Titanium Dioxide Nanocrystals for Enhanced Photonic Efficiencies, *J. Phys. Chem. C*, 2009, **113**, 7429–7435.

37 J. Yu, B. Yang and B. Cheng, Noble-metal-free carbon nanotube-Cd0.1Zn0.9S composites for high visible-light photocatalytic H_2-production performance, *Nanoscale*, 2012, **4**, 2670–2677.

38 A. F. Alkaim, Z. Sadik, D. K. Mahdi, S. M. Alshrefi, A. M. Al-Sammarraie, F. M. Alamgir, P. M. Singh and A. M. Aljeboree, Preparation, structure and adsorption properties of synthesized multiwall carbon nanotubes for highly effective removal of maxilon blue dye, *Korean J. Chem. Eng.*, 2015, **32**, 2456–2462.

39 S. Rather, N. Mehraj, R. Zacharia, S. W. Hwang, A. R. Kim and K. S. Nahm, Hydrogen storage of nanostructured TiO_2-impregnated carbon nanotubes, *Int. J. Hydrogen Energy*, 2009, **34**, 961–966.

40 J.-Y. Jung, D. Lee and Y.-S. Lee, CNT-embedded hollow TiO_2 nanofibers with high adsorption and photocatalytic activity under UV irradiation, *J. Alloys Compd.*, 2015, **622**, 651–656.

41 G. A. Tompsett, G. A. Bowmaker, R. P. Cooney, J. B. Metson, K. A. Rodgers and J. M. Seakins, The Raman spectrum of brookite, TiO_2 (Pbca, Z = 8), *J. Raman Spectrosc.*, 1995, **26**, 57–62.

42 H. Hiura, T. W. Ebbesen, K. Tanigaki and H. Takahashi, Raman studies of carbon nanotubes, *Chem. Phys. Lett.*, 1993, **202**, 509–512.

43 L. Grigorian, K. A. Williams, S. Fang, G. U. Sumanasekera, A. L. Loper, E. C. Dickey, S. J. Pennycook and P. C. Eklund, Reversible Intercalation of Charged Iodine Chains into Carbon Nanotube Ropes, *Phys. Rev. Lett.*, 1998, **80**, 5560–5563.

44 Z. I. Bedolla-Valdez, Y. Verde-Gomez, A. M. Valenzuela-Muniz, Y. Gochi-Ponce, M. T. Oropeza-Guzmand, G. Berhault and G. Alonso-Nuneza, Sonochemical synthesis and characterization of Pt/CNT, Pt/TiO_2, and Pt/CNT/TiO_2 electrocatalysts for methanol electro-oxidation, *Electrochim. Acta*, 2015, **186**, 76–84.

45 S. Santangelo, G. Faggio, G. Messina, E. Fazio, F. Neri and G. Neri, On the hydrogen sensing mechanism of Pt/TiO_2/CNTs based devices, *Sens. Actuators, B*, 2013, **178**, 473–484.

46 S. Santangelo, G. Messina, G. Faggio, A. Donato, L. De Luca, N. Donato, A. Bonavita and G. Neri, Micro-Raman analysis of titanium oxide/carbon nanotubes-based nanocomposites for hydrogen sensing applications, *J. Solid State Chem.*, 2010, **183**, 2451–2455.

47 W. Jarernboon, S. Pimanpang, S. Maensiri, E. Swatsitang and V. Amornkitbamrung, Effects of multiwall carbon nanotubes in reducing microcrack formation on electrophoretically deposited TiO_2 film, *J. Alloys Compd.*, 2009, **476**, 840–846.

48 N. Serpone, D. Lawless and R. Khairutdinovt, Size Effects on the Photophysical Properties of Colloidal Anatase TiO_2 Particles: Size Quantization versus Direct Transitions in This Indirect Semiconductor?, *J. Phys. Chem.*, 1995, **99**, 16646–16654.

49 K. Hemalatha, P. M. Ette, G. Madras and K. Ramesha, Visible light assisted photocatalytic degradation of organic dyes on TiO_2–CNT nanocomposites, *J. Sol-Gel Sci. Technol.*, 2015, **73**, 72–82.

50 Q. Xiang, J. Yu and P. K. Wong, Quantitative characterization of hydroxyl radicals produced by various photocatalysts, *J. Colloid Interface Sci.*, 2011, **357**, 163–167.

51 Y. Yang, L. Qu, L. Dai, T. S. Kang and M. Durstock, Electrophoresis Coating of Titanium Dioxide on Aligned Carbon Nanotubes for Controlled Syntheses of Photoelectronic Nanomaterials, *Adv. Mater.*, 2007, **19**, 1239–1243.

52 Y. Xu, M. Xie, T. Zhou, S. Yin, H. Xu, H. Ji, H. Li and Q. Zhang, In situ growth of Ag/AgCl on the surface of CNT and the effect of CNT on the photoactivity of the composite, *New J. Chem.*, 2015, **39**, 5540–5547.

53 Y. Zhang, D. Ma, J. Wu, Q. Zhang, Y. Xin and N. Bao, One-step preparation of CNTs/InVO4hollow nanofibers by electrospinning and its photocatalytic performance under visible light, *Appl. Surf. Sci.*, 2015, **353**, 1260–1268.

54 X. Li, Z. Zhuang, W. Li and H. Pan, Photocatalytic reduction of CO2 over noble metal-loaded and nitrogen-doped mesoporous TiO_2, *Appl. Catal., A*, 2012, **429–430**, 31–38.

55 K. Hashimoto, T. Kawai and T. Sakata, Photocatalytic reactions of hydrocarbons and fossil fuels with water. Hydrogen production and oxidation, *J. Phys. Chem.*, 1984, **88**, 4083–4088.

56 M. Ni, M. K. Leung, D. Y. Leung and K. Sumathy, A review and recent developments in photocatalytic water-splitting using TiO_2 for hydrogen production, *Renewable Sustainable Energy Rev.*, 2007, **11**, 401–425.

57 A. L. Linsebigler, G. Lu and J. T. Yates, Photocatalysis on TiO_2 Surfaces: Principles, Mechanisms, and Selected Results, *Chem. Rev.*, 1995, **95**, 735–758.

58 N. Li, Y. Ma, B. Wang, Y. Huang, Y. Wu, X. Yang and Y. Chen, Synthesis of semiconducting SWNTs by arc discharge and their enhancement of water splitting performance with TiO_2 photocatalyst, *Carbon*, 2011, **49**, 5132–5141.

59 D. E. Eastman, Photoelectric Work Functions of Transition, Rare-Earth, and Noble Metals, *Phys. Rev. B: Solid State*, 1970, **2**, 1–2.

60 F. J. Zhang and W. C. Oh, Comparison of the photonic effects of Mn-CNT/TiO_2 composites modified by different oxidants, *Kinet. Catal.*, 2011, **52**, 678–685.

61 K. Rajasekar, S. Thennarasu, R. Rajesh, R. Abirami, K. Balkis Ameen and A. Ramasubbu, Preparation of mesoporous TiO_2/CNT nanocomposites by synthesis of mesoporous titania via EISA and their photocatalytic degradation under visible light irradiation, *Solid State Sci.*, 2013, **26**, 45–52.

62 S. Suzuki, C. Bower, Y. Watanabe and O. Zhou, Work functions and valence band states of pristine and Cs-intercalated single-walled carbon nanotube bundles, *Appl. Phys. Lett.*, 2000, **76**, 4007–4009.

63 A. Kongkanand and P. V. Kamat, Electron Storage in Single Wall Carbon Nanotubes. Fermi Level Equilibration in Semiconductor – SWCNT Suspensions, *ACS Nano*, 2007, **1**, 13–21.

64 H. Kataura, Y. Kumazawa, Y. Maniwa, I. Umezu, S. Suzuki, Y. Ohtsuka and Y. Achiba, Optical properties of single-wall carbon nanotubes, *Synth. Met.*, 1999, **103**, 2555–2558.

65 A. Fujiwara, Y. Matsuoka, H. Suematsu, N. Ogawa, K. Miyano, H. Kataura, Y. Maniwa, S. Suzuki and Y. Achiba, Photoconductivity of single-wall carbon nanotube films, *Carbon*, 2004, **42**, 919–922.

66 U. Coscia, G. Ambrosone, A. Ambrosio, M. Ambrosio, F. Bussolotti, V. Carillo, V. Grossi, P. Maddalena, M. Passacantando, E. Perillo, A. Raulo and S. Santucci, Photoconductivity of multiwalled CNT deposited by CVD, *Solid State Phys.*, 2009, **11**, 1806–1809.

67 K. Dai, X. Zhang, K. Fan, T. Peng and B. Wei, Hydrothermal synthesis of single-walled carbon nanotube-TiO_2 hybrid and its photocatalytic activity, *Appl. Surf. Sci.*, 2013, **270**, 238–244.

68 Y. T. Park, A. Y. Ham and J. C. Grunlan, High Electrical Conductivity and Transparency in Deoxycholate-Stabilized Carbon Nanotube Thin Films, *J. Phys. Chem. C*, 2010, **114**, 6325–6333.